Oligomeric assembly and interactions within human RuvBL1 and RuvBL2 complexes

Andrew Niewiarowski, Alison S Bradley, Jayesh Gor, Adam R. Mckay, Stephen J. Perkins, Irina R Tsaneva

Oligomeric assembly and interactions within human RuvBL1 and RuvBL2 complexes

Andrew Niewiarowski[1], Alison S. Bradley[1], Jayesh Gor[1], Adam R. McKay[2], Stephen J. Perkins[1] and Irina R. Tsaneva[1*]

[1] Department of Structural and Molecular Biology, Darwin Building, University College London, Gower Street, London WC1E 6BT, U. K.

[2] Department of Chemistry, University College London, 20 Gordon Street, London WC1H 0AJ, U. K.

Corresponding Author: Irina R Tsaneva Tel: 020-7679-2235; Fax: 020-7679-7193; email: tsaneva@biochemistry.ucl.ac.uk.

Short Title: Assembly of RuvBL1 and RuvBL2 complexes

Keywords: RuvBL1 (TIP49, Pontin); RuvBL2 (TIP48, Reptin); AAA+ proteins; oligomerisation: analytical ultracentrifugation; Mass spectrometry.

Abbreviations: AAA+, ATPases associated with various cellular activities; AUC, analytical ultracentrifugation; MS, mass spectrometry; SEC, size exclusion chromatography; Δ, Domain II deletion mutant.

SYNOPSIS

The two closely related eukaryotic AAA^+ proteins, RuvBL1 (TIP49) and RuvBL2 (TIP48), are essential components of large multi-protein complexes involved in diverse cellular processes. While the molecular mechanisms of RuvBL1 and RuvBL2 remain unknown, oligomerization is likely to be important for their function together or individually and different oligomeric forms might underpin different functions. Several experimental approaches were used to investigate the molecular architecture of the RuvBL1/2 complex and the role of the ATPase-insert domain (Domain II) for its assembly and stability. Analytical ultracentrifugation showed that RuvBL1 and RuvBL2 were mainly monomeric and each co-existed with small proportions of dimers, trimers and hexamers. Adenine nucleotides induced hexamerisation of RuvBL2 but not RuvBL1. In distinction, the RuvBL1/2 complexes contained single and double hexamers together with smaller forms. The role of the ATPase-insert domain (Domain II) in complex assembly was examined by size exclusion chromatography using deletion mutants of RuvBL1 and RuvBL2. Significantly, catalytically competent dodecameric RuvBL1/2 complexes lacking Domain II in one or both proteins could be assembled but the loss of Domain II in RuvBL1 destabilised the dodecamer. The composition of the RuvBL1/2 complex was analysed by mass spectrometry. Several species of mixed RuvBL1/2 hexamers with different stoichiometries were seen in the spectra of the RuvBL1/2 complex. A number of our results indicate that the architecture of the human RuvBL1/2 complex does not fit the recent structural model of the yeast Rvb1/2 complex.

INTRODUCTION

RuvBL1 (TIP49, Pontin) and RuvBL2 (TIP48, Reptin) are two highly conserved eukaryotic AAA$^+$ proteins (ATPases associated with various cellular activities) that are engaged in a number of functionally important protein-protein interaction networks in all eukaryotic organisms[1-3]. The nomenclature standardisation following publication of the Human Genome adopted the names "RuvB-like" due to their structural homology to the bacterial Holliday junction branch migration protein RuvB. Nevertheless, they are functionally distinct from RuvB [4-7] and are implicated in several diverse cellular functions. RuvBL1 and RuvBL2 are individually essential in all eukaryotes [6, 8-9] and are involved in transcriptional regulation and chromatin remodelling [10-12], DNA repair [4, 13], snoRNP biochemistry [14-15], telomerase activity [16] and mitotic spindle assembly [17-19]. Several of the pathways employing RuvBL1 and RuvBL2 are directly involved in cancer development including the β-catenin/Wnt signalling pathway and cMyc [20-21]. RuvBL1 and RuvBL2 are deregulated in several clinical cases of cancer but the role of RuvBL1 and RuvBL2 activity is not well understood [21].

RuvBL1 and RuvBL2 participate in large multi-subunit complexes that include proteins such as INO80[12], SRCAP [22], URI1[23] , Box C/D snoRNP complexes[15] and TIP60 [4]. RuvBL1 and RuvBL2 are often present together in a 6:1 molar ratio relative to other proteins in these complexes [12] suggesting that both function as hexamers. Interestingly, the abundance of RuvBL1 and RuvBL2 in eukaryotic cells relative to other components of these complexes is too low for them to be permanently associated with each complex [2]. This suggests a transient function in complex assembly rather then direct catalytic activity. Indeed, *S. cerevisiae* RuvBL1 (Rvb1p) and RuvBL2 (Rvb2p) are needed for the correct assembly of the INO80 complex by recruiting Arp5p [24]. RuvBL1 and RuvBL2 are required for the restructuring of the box C/D snoRNP complex [15] and the assembly of active telomerase complex [16]. RuvBL1 and RuvBL2 activities may not always involve co-operation between the two proteins and may act independently and in opposing fashion [8, 25-26]. Complexes containing one of the proteins without the other were also identified [27] and RuvBL2 shows distinct localisation during mitosis [19]. To date, no specific mechanism of action has been attributed to RuvBL1 and RuvBL2.

The hexamer or double hexamer structure is a typical feature of AAA$^+$ proteins which is necessary for catalytic function [28-29]. The crystal structure of human RuvBL1 showed the classic AAA$^+$ hexameric ring with the ATP binding sites at the subunit interfaces [7]. The three domains in RuvBL1 are two 'RuvB like' Domains I and III which formed the core hexameric ATPase ring, and a third, Domain II, which is not found in RuvB. Domain II is incorporated between the Walker A and B motifs within Domain I [7, 30]. Interestingly, the nucleotide binding pockets occupied by ADP were enclosed in the RuvBL1 hexamer crystal structure, suggesting that a restructuring event is needed for the release of hydrolysed ATP. The weak ATPase activity of RuvBL1 and RuvBL2 *in vitro* increased synergistically when the proteins formed a double hexameric complex [4-5] showing that this is the enzymatically-active form. The human RuvBL1/2 complex showed two tightly packed and structurally distinct hexameric rings by negative stain electron microscopy

[5]. A very different structure for the yeast Rvb1/Rvb2 complex was obtained by cryo-electron microscopy [31]. The yeast model placed the two hexameric rings in an extended head-to-head orientation, in which Domain II formed the interface between the rings. Immuno-labelling of the yeast double hexamer complex argued against the presence of mixed hexamers [31]. However, a different electron microscopy study of yeast RuvBL1/2 showed a mixed single hexameric complex [32].

The discrepancies between the human and yeast structures suggest that RuvBL1 and RuvBL2 may form structurally distinct complexes. To investigate the different oligomeric forms of the human RuvBL1/2 proteins and the architecture of their complex we used size exclusion chromatography (SEC) analytical ultracentrifugation (AUC) and mass spectrometry (MS). Using sedimentation velocity as a quantitative tool, we show that individually ligand-free RuvBL1 and RuvBL2 are monomeric and that RuvBL2 forms a hexamer in the presence of nucleotide. Molecular modelling of the AUC data revealed that RuvBL1/2 complexes were comprised of monomeric, dimeric, trimeric, hexameric and dodecameric species. Mass-spectrometry provided direct evidence that the complex contained mixed hexamers with varying stoichiometries. In these studies we also used mutants of RuvBL1 and RuvBL2 without the globular region of Domain II. The deletion mutants could form double hexamers but the deletion of RuvBL1 Domain II destabilised the double hexamer. Mixed hexamers with different stoichiometries were also identified in the deletion mutants. In summary, we show that RuvBL1/2 exists in a series of oligomeric forms, whose assembly could be regulated by Domain II. Our findings about the human RuvBL1/2 complex cannot easily fit the recent structural model of the yeast Rvb1/2 complex.

EXPERIMENTAL

Protein expression and purification

His_6-RuvBL1 was expressed using the pET15-His_6-RuvBL1 expression plasmid in BL21-Gold (DE3) *E. coli* and purified by Talon (Clontech) metal affinity and hydroxylapatite column chromatography [5]. RuvBL2-His_6 was expressed using the pET21-RuvBL1-His_6 expression plasmid in BL21-Gold (DE3) *E. coli* and purified using Talon metal affinity and MonoQ column chromatography [5]. For coexpression of the RuvBL1-His_6/RuvBL2 complex, a pET21-based plasmid encoding both RuvBL1-His_6 and RuvBL2 was transformed into BL21 Rosetta II (DE3) *E. coli*. After protein expression [5], the soluble lysate was applied to a Talon column. RuvBL1-His_6 and RuvBL2 were both captured and eluted at around 50 – 150 mM imidazole using 0 to 250 mM gradient. The proteins were dialysed into R buffer (20 mM Tris HCl pH 8, 100 mM NaCl, 1 mM phenylmethylsulphonyl fluoride, 1 mM dithiothreitol, 10 % glycerol) and supplemented with either 1 mM EDTA or 2 mM $MgCl_2$. The sample was passed through a ssDNA cellulose column; the flow through was concentrated to 0.5 ml using Amicon ultra 10 kDa exclusion centrifugal concentrators (Millipore), then further purified by SEC on a Superose 6 HR column.

Domain II deletion mutant constructs and purification

pET15-His_6-ΔRuvBL1, pET21-ΔRuvBL2-His_6 and pET21-based coexpression plasmids were generated from the wild type constructs by a single step PCR reaction using the Phusion site directed mutagenesis kit (Finnzymes). Primers were designed so that residues Glu-126 to Ile-234 inclusive were removed from ΔRuvBL1 and residues Glu-133 to Val-238 inclusive were removed from ΔRuvBL2. Deletion of the entire Domain II of RuvBL1 as defined by the crystal structure (residues 121 – 295) resulted in totally insoluble protein as reported [7]. The missing residues were replaced with Ala-Gly-Ala in the resulting recombinant proteins.

Size exclusion chromatography (SEC)

Proteins were dialysed against R buffer with 1 mM EDTA or 2 mM $MgCl_2$ and incubated for 20 min on ice with 1 mM ATP when required. The samples (up to 5 mg of protein in 500 µl) were filtered through 0.2 µm syringe filters (Millipore), loaded on Superose 6 HR column and eluted in R buffer (with 1 mM EDTA or 2 mM $MgCl_2$ with 0.1 mM ATP as required). Absorbance profiles were detected at 280 nm, 1 ml fractions were collected and analysed by 12 % SDS PAGE. Protein molecular weights were estimated by comparison with five standards (Biorad) and Dextran blue. Fraction 15 from the SEC purification of RuvBL1/2 was reapplied to the Superose 6 column in R buffer with no EDTA. Fractions 14-16 obtained were incubated with 200 µl of Talon resin for 30 mins at 4 ºC with mild agitation. The resin was washed twice with Talon buffer and the protein was eluted for SDS-PAGE analysis by incubating the resin with 500 µl of Talon buffer supplemented with 200 mM imidazole for 10 min at 4 ºC.

Reconstitution of RuvBL1/2 complex.

0.8 mg of each His_6-RuvBL1 and RuvBL2-His_6 (from the 70 kDa fraction) were mixed in 10 ml R buffer containing 1 mM EDTA and incubated for 15 min on ice. To test the effect of ATP 0.8 mg of RuvBL2-His6 in R buffer were supplemented with 5 mM $MgCl_2$ and 1 mM ATP. Following incubation for 15 min on ice, 0.8 mg of His_6-RuvBL1 was added to a final volume of 10 ml. Both mixtures were concentrated to 0.5 ml and fractionated by SEC on Superose 6 HR column

Analytical ultracentrifugation (AUC) data and analyses

RuvBL1, RuvBL2 and the RuvBL1/2 complex were dialysed extensively against one of four different AUC buffers supplemented with cofactors as required: (i) The EDTA buffer was comprised of 20 mM Tris-HCl pH 8, 200 mM NaCl, 0.1 mM dithiothreitol, 0.1 mM EDTA; (ii) the magnesium buffer was 20 mM Tris-HCl pH 8, 200 mM NaCl, 0.1 mM dithiothreitol, 2 mM $MgCl_2$ to which was added either (iii) 0.5 mM ATP or (iv) 0.5 mM ADP when preparing the ATP and ADP buffers respectively. Buffer densities and viscosities of 1.0072 g/ml and 0.01027 cp for the four buffers were calculated from compositions using SEDNTERP [33]. ADP and ATP were added after sample dialysis. Protein concentrations were determined either from Bradford assays using bovine serum albumin as a standard or from 280 nm absorption coefficients of 3.49 for RuvBL1, 3.64 for RuvBL2 and 3.57 for their complex (1%, 1 cm path length) calculated from compositions [34].

Sedimentation velocity runs were performed using Beckman Optima XL-I analytical ultracentrifuges at 20 °C using an AnTi50 rotor. Absorbance and interference data sets were collected at rotor speeds of 25,000, 30,000, 35,000 and 42,000 r.p.m. for RuvBL1 and RuvBL2, and 25,000 and 30,000 r.p.m. for the RuvBL1/2 complex in two sector cells with column heights of 12 mm. The different rotor speeds established the absence of rate exchange or rotor speed effects on the sedimentation coefficient ($s^0_{20,w}$) analyses [35]. Scans were recorded at 8 min intervals until sedimentation was complete. Molecular masses and partial specific volumes of 52.4 kDa and 0.747 ml/g for RuvBL1, 52.1 kDa and 0.743 ml/g for RuvBL2, and 102.5 kDa and 0.745 ml/g for the RuvBL1/2 complex were calculated from compositions [34]. Sedimentation analysis was performed using direct boundary Lamm fits of 70 to 110 absorbance or interference scans using SEDFIT (version 9.4b) [36]. SEDFIT resulted in size distribution *c(s)* analyses that assumed that all the observed species have the same frictional ratio (f/f_0). The analysis of *c(s)* fits for oligomeric species followed previous procedures [37].

Hydrodynamic modelling of sedimentation coefficients

RuvBL1 and RuvBL2 oligomers were modelled using the crystal structure of the human RuvBL1-ADP complex (PDB code 2c9o) [7]. Hexamer 1 was generated from monomer A in spacegroup P6, using the Protein Quaternary Structure website at http://pqs.ebi.ac.uk/. Hexamer 1 showed that an accessible surface area of 4102 $Å^3$ (15.8% of the total) was lost on hexamer formation, and all six monomers were in the same symmetric orientation around the hexameric ring. Up to 10 salt bridges between each monomer and its two neighbours occurred between Arg14-Asp353, Lys107-Glu105, Arg339-Asp343 and Arg404-Asp356. The symmetry operators for the six monomers were defined by X, Y, Z; Y,-X+Y, Z; X-Y, X, Z; -X+Y,-X, Z; -Y, X-Y, Z;

and -X, -Y, Z. Hexamer 2 was generated by alternating the orientation of monomers B and C around the ring. Monomer, dimer, trimer, hexamer, nonamer and dodecamer structures were created using INSIGHT II 98.0 molecular graphics software (Accelrys, San Diego, CA, USA) on Silicon Graphics OCTANE Workstations. The $s^0_{20,w}$ values were calculated directly from atomic coordinates using HYDROPRO with the default value of 0.31 nm for the atomic element radius to represent the hydration shell [38]. The agreements between experimental and predicted $s^0_{20,w}$ values are generally within 0.3 S [39].

The electron microscopy structure for the RuvBL1/2 complex at 20 Å resolution was downloaded from the 3D-EM electron microscopy database (deposition code 1317) at http://www.ebi.ac.uk/msd/projects/IIMS.html [5]. This was converted into SPIDER format using EM2EM software at http://www.imagescience.de/em2em/. A pixel size of 3.3 Å and a density cut-off threshold of 0.547 generated a volume of 728,000 Å^3 close to the sequence-derived volume of 751,000 Å ^{3} for the RuvBL1/2 complex. The $s^0_{20,w}$ value was calculated using HYDROMIC [40].

ATPase assays

Assays were carried out using the P_i ColorLock ALS colourimetric kit (Innova Biosciences). Reactions were carried out in a final volume of 200 µl in ATPase Buffer (50 mM Tris pH 8, 100 mM NaCl, 0.1 mg/ml bovine serum albumin, 2 mM $MgCl_2$, 0.5 mM ATP). To start the reactions, 20 µl of material from each fraction eluted from the Superose 6 column were added and the reactions were incubated at 37 ºC for 30 minutes. After 30 min, 20 µl from each reaction was added to 5 µl of 0.5 M EDTA pH 8.5 in 96 well round bottomed tissue culture test plates (Techno Plastic Products) in triplicate. 125 µl of ALS malachite green solution were added to each well, the colour was left to develop for 30 min, and then the absorbance at 635 nm was measured using a Tecan Sunrise microplate absorbance reader. 20 µl of different concentrations of KP_i were also measured as above to generate a standard curve.

Mass Spectrometry (nanoESI MS) data and analyses

Proteins were buffer-exchanged into 250 mM ammonium acetate at pH 7.5 by SEC on a Superdex 200 10/300 gel filtration column. SEC fractions were pooled and concentrated using Vivaspin 2mL centrifugal concentrators with a molecular weight cut off of 10 kDa (Sartorius, Aubagne Cedex, France) to a final concentration of approximately 20 uM.

Mass spectrometry measurements were carried out on a Synapt HDMS mass spetrometer. (Waters, Manchester, UK). Nanoflow electrospray ionization of protein samples was performed using gold coated glass capillaries prepared in house. Typical conditions employed 2-3 uL of aqueous protein solution, capillary voltages of 1.1-1.5 kV, cone voltages of 50-80 V, trap and transfer collison energies of 30 and 10 V respectively. For CID-induced activation, the trap collision voltage was varied during the acquisition of spectra while keeping other settings constant. External calibration was achieved by using a 33 mg/ml aqueous solution of cesium iodide (Sigma, St. Louis, MO, USA).

RESULTS

Purification of RuvBL1, RuvBL2 and the RuvBL1/RuvBL2 complex

RuvBL1 and RuvBL2 were expressed in *E. coli* and purified (Experimental). In agreement with our previous data, RuvBL1 was monomeric under all conditions tested by size exclusion chromatography (SEC), whereas RuvBL2 underwent adenine nucleotide-dependent oligomerisation [5]. This intrinsic difference between the two proteins could not be attributed to their hexahistidine tags for two reasons. Firstly, identical elution profiles were observed with RuvBL1 tagged at the C- or N-terminus ([5] and this study). Secondly, in the presence of 250 mM imidazole, RuvBL2-His_6 was still a mixture of hexamers and monomers similar to samples analysed in the absence of imidazole (data not shown).

RuvBL1-His_6 and untagged RuvBL2 were co-expressed in *E. coli*. The complex was captured on metal affinity column and further fractionated by SEC (Experimental). A major species of approximately 617 kDa was eluted, in good agreement with the predicted molecular weight of a dodecamer of 622 kDa (Figure 1 A), together with an excess of monomeric RuvBL1 at 55 kDa and a range of intermediate species. The two main fractions of the RuvBL1/2 complex (13 and 14) were pooled and re-applied to the column at different dilutions (Figure 1 B). At all concentrations, the complex eluted at exactly the same volume which indicates that the dodecameric complex did not undergo concentration-dependent disassembly under these conditions. The effect of ATP on the RuvBL1/2 complex was also examined. The peak fraction of the dodecamer was incubated with EDTA or with Mg-ATP, then analysed by SEC (Experimental). Upon incubation with Mg-ATP, the dodecameric peak was still prominent but a new peak appeared (Figure 1 C). This indicates partial dissociation of the dodecamer following incubation with ATP but the species formed would be difficult to assess using SEC.

Interestingly RuvBL1 and RuvBL2 co-eluted down to fraction 15 which corresponds to a hexamer (Figures 1 A). When re-applied to the column fraction 15 still eluted as a hexamer (Figures 1 D and E). Both RuvBL1-His_6 and the untagged RuvBL2 in the hexamer fractions could be captured on Talon resin (Talon in Figure 1 E) which shows the presence of a mixed RuvBL1/2 oligomer, presumably a hexamer. A slight excess of RuvBL1 can be noted in the fractions but a precise stoichiometry is difficult to derive due to the low protein concentration. The analysis of the RuvBL1/2 complex by SEC revealed a heterogeneous population of oligomers but the predominant species in Figure 1 A is the double hexamer. It also displayed the highest ATPase activity (see below) and is therefore most likely to be the enzymatically active form of the complex.

Analytical ultracentrifugation identifies several oligomers of RuvBL1 and RuvBL2 and their complex

The qualitative nature of SEC in observing effective hydrodynamic radii means that the number of subunits in the oligomers of RuvBL2 could not be accurately assigned. To elucidate further details on the assembly of the RuvBL1/2 complex, analytical ultracentrifugation (AUC) was performed. Sedimentation velocity data were collected for RuvBL1 and RuvBL2 in EDTA at concentrations between 0.1

– 2.0 mg/ml and 0.1 – 1.5 mg/ml respectively at four rotor speeds. SEDFIT analyses of the interference optics data fit all the scans to determine the size distribution function *c(s)*. For RuvBL1 in EDTA, the *c(s)* plots reproducibly showed at least four discrete species. The equivalent data sets from absorbance optics measured in the absence of nucleotides (which absorb strongly at 280 nm) were closely similar (data not shown). The major peak was consistently observed at 2.9 – 3.1 S, and three additional peaks at 4.5 – 5.0 S, 6.5 – 7.0 S and 10.0 – 10.5 S successively decreased in intensities (Figure 2 A). Importantly, the peak positions were unchanged with RuvBL1 concentration or with rotor speed (Figure 3), indicating that any exchange rate processes between the oligomers are slow on the time-scale of sedimentation, and in turn indicating that stable species have been observed. Assuming that the same frictional ratio *f/fo* of 1.36 ± 0.22 is applicable to all the peaks, the conversion of the *c(s)* curves to mass distribution *c(M)* curves showed that these species corresponded to monomer, dimer, trimer and hexamer forms respectively. Good agreement within error was obtained between each peak mass and the protein sequence mass (Table 1). In agreement with previous SEC analyses [5] integrations of the *c(s)* peaks showed no significant change in their relative proportions when RuvBL1 was incubated with 0.5 mM ADP or ATP in the presence of 2 mM Mg^{2+} (Figure 2 B; ADP data not shown), even though the different peak widths and heights in Figures 2 A and B may suggest otherwise.

The *c(s)* analyses of the interference data for RuvBL2 collected in 0.1 mM EDTA, revealed the same four peaks as for RuvBL1 (Figure 2 C). The 2.9 – 3.1 S peak was again the principal species, and minor peaks were observed at 4.5 – 5.0 S, 6.5 – 7.0 S and 10.0 – 10.5 S (Table 1). No dependence of the peaks on concentration or rotor speed was again observed (Figure 3). These were assigned as monomers, dimers, trimers and hexamers from the *c(M)* analyses (Table 1). In marked distinction to RuvBL1, the pre-incubation of RuvBL2 with either 0.5 mM ADP or ATP in 2 mM $MgCl_2$ caused the hexamer peak at 10.0 – 10.5 S to become predominant, together with much reduced intensities of the monomer, dimer and trimer peaks (Figures 2 D; ADP data not shown). Thus, both ADP and ATP in the presence of $MgCl_2$ induced RuvBL2 to form hexamers. We conclude that the previously observed 70 and 400 kDa species for RuvBL2 by SEC [5] corresponded to a mixture of monomer/dimers and hexamers respectively.

The RuvBL1/2 complex was analysed by AUC using the high molecular weight fractions between 12.5 ml to 14.5 ml from SEC (Figure 1 A). Velocity data using interference optics were collected at concentrations of 0.1 – 0.8 mg/ml. The *c(s)* analyses for the RuvBL1/2 complex in EDTA showed a series of oligomers (Figure 2 E). No concentration or rotor speed dependence of the peaks was seen (Figure 3). The 3.0 – 3.3 S peak was attributed to the monomer of either RuvBL1 or RuvBL2. Prominent peaks at 4.5 – 5.0 S, 6.5 – 7.0 S and 10.0 – 10.5 S were attributed to dimers, trimers and hexamers (Table 1). A major new peak now appeared at approximately 18.3 S, which corresponded to a larger RuvBL1/2 complex (Figure 2 E). An intermediate peak between the 10.3 S and 18.3 S peaks was difficult to measure accurately due to poor resolution. Since the pre-formed RuvBL1/2 complex had been isolated using SEC, the observed separate species indicates the partial dissociation of the complex during ultracentrifugation. As with the SEC experiments (Figure 1 C), the presence of 0.5 mM ADP or ATP in 2 mM $MgCl_2$ notably increased the relative proportion of hexamer at 10.3 S, although the 18.3 S peak was still

prominent (Figure 4 F). This outcome can be attributed to dissociation of the dodecamer into hexamers. Hexamer formation of free RuvBL2 in the presence of ADP or ATP could also contribute to this peak but the level of free RuvBL2 in the starting material would be too low to explain the effect observed (Figure 2 D).

For the RuvBL1/2 complex, the *c(M)* plots showed molecular weights that were 30-70% higher than expected (Table 1). This increase was attributed to a 30% increase in the fitted frictional ratio *f/fo* to 1.76 ± 0.23 for the RuvBL1/2 complexes compared to the individual proteins. This change may reflect the more complicated shapes of the higher oligomers (see below). Accordingly, while the s values remained similar for RuvBL1, RuvBL2 and their complexes, the *c(M)* masses were not able to identify the oligomer stoichiometry for the complex.

Confirmation of sedimentation coefficients by modelling

Sedimentation coefficients were calculated from the RuvBL1 crystal structure [7] in order to confirm the *c(s)* analyses (Figure 4). Sequence and secondary structure comparisons indicated that the RuvBL1 and RuvBL2 structures were very similar. Thus RuvBL2 contained 463 residues, only 13 more than RuvBL1. Residue conservation is high at 42% between the two sequences, especially in the secondary structural regions seen in the RuvBL1 crystal structure. Two alternative hexamers could be generated from the RuvBL1 crystal structure. Hexamer 1 corresponds to six copies of monomer A in the same orientation, while Hexamer 2 corresponds to monomers B and C in alternating orientations (Experimental). Hexamers 1 and 2 differ mainly in the location of the extended Domain II region, which is most likely to result from different crystal packing. Hexamer 1 gave predicted sedimentation coefficients of 3.3 S, 5.2 S, 6.8 S and 10.6 S for the monomer, dimer, trimer and hexamer forms of RuvBL1 respectively. Hexamer 2 gave slightly higher predicted values. These agree well with the observed S values for RuvBL1 and RuvBL2 (Table 1).

The sedimentation coefficient of the dodecamer was calculated from Hexamer 1 and the electron microscopy reconstruction of the RuvBL1/2 complex [5]. Hexamer 1 is most compactly arranged in a head-to-tail configuration (Figure 4). From this, the predicted sedimentation coefficient of 18.4 S agrees with the observed value of 18.4 S. Such a head-to-tail arrangement would account for the existence of even higher oligomers such as an 18-mer, and would account for additional features seen in Figure 1 A at high mass and in Figures 2 E and F at high S. The electron microscopy model gave a predicted sedimentation coefficient of 19.0 S, also in good agreement with the experiment. Thus, we conclude that the sedimentation coefficient for the dodecamer is well explained by modelling.

The Domain II-deletion mutants of ΔRuvBL1 and ΔRuvBL2 form double hexameric complexes

The above modelling results are consistent with a head-to-tail configuration of the double hexameric complex but cannot prove this model. In the head-to-head model proposed [31] the interface between the two hexamers involves interactions between Domain II. To assess the importance of Domain II for the RuvBL1/2 complex, mutants lacking Domain II (Δ) were engineered. Soluble proteins were

generated when the deletions retained a part of Domain II considered to be necessary for Domain I to fold correctly and were 12 kDa smaller than the full-length protein. Residues Glu126 to Ile234 (α-carbon separation of 5.3 Å) for ΔRuvBL1-His_6, and Glu133 to Val238 for His_6-ΔRuvBL2 were replaced with a flexible Ala-Gly-Ala linker. These residues occur at the centre of the two long β-strands that connected the bulk of Domain II to Domain I (Figure 5).

The deletion mutants of RuvBL1 and RuvBL2 were analysed individually by SEC. Similar to the wild type protein, ΔRuvBL1 eluted as monomer of 40 kD and was not affected by Mg-ATP (data not shown). In EDTA ΔRuvBL2 eluted as a monomer at 45 kDa, a probable hexamer at 220 KDa and a range of higher molecular mass species. Unlike the full-length RuvBL2, incubation of ΔRuvBL2 with Mg-ATP had no effect on the elution profile (Figure 5A) but concentration-dependent changes in the ΔRuvBL2 oligomers were observed (Figure 5B). These observations implicate the globular region of Domain II of RuvBL2 in regulating the nucleotide-dependent oligomerization of RuvBL2.

Three different RuvBL1/2 complexes containing one or both of the deletion mutants were examined. The complexes of ΔRuvBL1/RuvBL2, RuvBL1/ΔRuvBL2 and ΔRuvBL1/ΔRuvBL2 were captured on a Talon column, fractionated by SEC and ATPase activity was measured across the eluted fractions. As a benchmark, the full-length RuvBL1/2 complex eluted predominantly as a double hexamer at about 617 kDa, which displayed the highest ATPase activity; the free RuvBL1 monomer had little activity (Figure 6 A and C). The elution profiles of the mutant complexes each contained a prominent dodecamer peak (Figures 6 D, G, and J). The molecular masses calculated were all were consistent with the expected values of a double hexamer. In sedimentation velocity experiments, the *c(s)* plots for RuvBL1/ΔRuvBL2 and ΔRuvBL1/ΔRuvBL2 displayed both hexamer and double hexamer peaks (data not shown). These results demonstrate that the globular region of Domain II is not essential for double hexamer formation. Moreover, the peak ATPase activity was consistently observed in the fractions corresponding to double hexamers (Figures 6 F, I and L).

While the deletion of Domain II of RuvBL2 had no affect on the dodecameric complex, that of RuvBL1 clearly did. The RuvBL1/ΔRuvBL2 complex was exclusively dodecameric and virtually identical to the full-length complex (compare Figure 6 G and A). This shows that the globular region of RuvBL2 Domain II is not engaged in contacts between the two hexameric rings. However, the elution profiles of both ΔRuvBL1/2 and ΔRuvBL1/ΔRuvBL2 showed a clear second peak corresponding to a hexamer (Figures 6 D and J). The appearance of hexamers indicates that unlike RuvBL2, Domain II of RuvBL1 contributes to stable contacts between the two rings in the double hexamer.

Reconstitution of RuvBL1/2 complexes and effect of ATP-Mg.

The results presented above could not distinguish between RuvBL1/2 complexes consisting of homo- or heterohexamers. We wanted to test whether nucleotide-induced hexamerization of RuvBL2 would act as a scaffold for RuvBL1 hexamerisation thereby facilitating the assembly of RuvBL1/2 complex made of homohexamers. Complexes were assembled from purified RuvBL1 and RuvBL2 in

EDTA or Mg-ATP and analysed by SEC (Experimental). The complex reconstituted in EDTA eluted with a peak at 13.4 ml at the position of the double hexamer (Figure 7). Both proteins coeluted in the high molecular fractions along with some monomeric RuvBL1. Even though the protein levels were very similar in the starting mixture, a slight excess of RuvBL2 could be seen in the heavy fractions. The complex reconstituted in the presence of Mg-ATP eluted with a peak at 14.1 ml, shifted towards the position of a hexamer, and the two proteins showed clear equimolar ratios in all oligomeric fractions (Figure 7 C). The predominance of the hexamers in Mg-ATP could be due to dissociation of the double hexamers as seen by SEC and AUC (Figure 1 and 2). It is worth noting that the reported yeast Rvb1/2 mixed hexamers were formed in the presence of different adenine nucleotides [32]. The reconstitution experiments in Mg-ATP argue against a role for a preformed RuvBL2 hexameric ring acting as a scaffold for the formation of a second RuvBL1 hexamer. The results are consistent with the formation of mixed hexamers, in agreement with mass spectrometry data (below). They also suggest that ATP binding and/or hydrolysis facilitate the interactions between RuvBL1 and RuvBL2 and could regulate the assembly of equimolar complexes.

Mass spectrometry of the RuvBL1/RuvBL2 and ΔRuvBL1/ΔRuvBL2 high molecular weight fraction reveals heterogenous poulations of mixed hexamers.

The composition of the hexamers in the RuvBL1/2 complex could be probed directly using mass spectrometry. All experimental and theoretical masses are summarized in Table 2. The NanoESI MS spectrum of the RuvBL1/RuvBL2 complex was obtained after separation of the hexameric fraction by SEC on a Superdex 200 column (Figure 8 A). A well resolved charge state series was obtained centred on 8250 *m/z*. Prior to comparison with experiment, theoretically calculated masses from the protein sequences were corrected for the presence of salt and solvent adducts [41]. The ion series has a measured mass of 313,682 ± 40 Da which is consistent with that expected for a 4:2 stoichiometry of RuvBL1/RuvBL2 suggesting that both RuvBL1 and RuvBL2 monomers are present in the hexamer. Interestingly a second smaller ion series is also visible in the spectrum centred on 8197 *m/z*. (Figure 8 A, asterisk) This has a mass consistent with 3:3 stoichiometry of RuvBL1/RuvBL2. The presence of a second ion series with a mass corresponding to an alternative stoichiometry of the RuvBL1/RuvBL2 hexamer indicates that heterogenous populations of RuvBL1/RuvBL2 complexes can form in solution.

In order to confirm the stoichiometry assignment and determine if both RuvBL1 and RuvBL2 monomers are present in the hexameric species, we employed tandem mass spectrometry. Here the quadrupole mass analyzer of the tandem MS instrument is used as a filter to isolate a single charge state of the hexameric complex, which is then subjected to energetic collisions with argon atoms to affect fragmentation. Previously such experiments have demonstrated that protein complexes fragment via the unfolding and dissociation of a protein monomer in a charge asymmetric fashion. This produces highly charged monomeric protein ions at low *m/z* and charge deficient fragments of the remaining complex at high *m/z* [42-45]. The tandem MS spectrum of the 39+ charge state of the proposed 4:2 RuvBL1/RuvBL2 complex produces three such related fragment ion families (Figure 8 B). The two ion series labelled (1) in the spectrum result from the fragmentation of the 39+ hexameric ion to produce highly charged RuvBL1 monomer ions centred on

2020 *m/z* and ions from a pentameric RuvBL1/RuvBL2 complex with a stoichiometry of 3:2. Similarly, the peak series marked (2) results from the fragmentation of the 39+ charge state of the 4:2 hexamer to produce highly charged RuvBL2 monomer ions centred on 2040 m/z and and ions from a pentameric RuvBL1/RuvBL2 complex with a stoichiometry of 4:1. The final ion series labelled (3) represents the loss of a 9 kDa fragment of one of the RuvBL proteins. This could have arisen from protease activity on the assembled complex but due to an absence of a 9kDa band in SDS gels, it is believed that this fragment may have arisen from covalent fragmentation of an N-terminal portion of RuVBL1 at position 95 (C/P residues) in competition with noncovalent dissociation. This behaviour has been observed before, in high energy collisions of noncovalent complexes in surface induced dissociation and is particularly favoured at proline residues [46].

Similar experiments were performed on the hexameric fraction of the ΔRuvBL1/ΔRuvBL2 complex (Figure 8C). Again a well resolved ion series is obtained. The predominant ion series is centred on 7115 *m/z* and also has a mass consistent with a 4:2 stoichiometry of ΔRuvBL1/ΔRuvBL2. In this case a total of three ion series are distinguishable and are visible in the expansion of the spectrum (inset) labeled (a-c) on the 35+ charge state and are consistent with 3:3, 4:2 and 5:1 stoichiometries of ΔRuvBL1 to ΔRuvBL2 respectively. Tandem MS experiments of the ΔRuvBL1/ΔRuvBL2 complex also confirmed the presence of both proteins in the hexameric complex. The simultaneous presence of mixed hexamers with different stoichiometries in both the full length and the deletion complexes may explain the difficulties in crystallising these complexes.

The 4:2 stoichiometry of the hexamers observed was surprising but was consistent with the slight excess of RuvBL1 over RuvBL2 observed in some of the preparations (e.g., Figure 1E, Figure 7A). It may be that the stoichiometry of the two proteins varied from one preparation to the next, which could be due to differences in expression levels of the two proteins. Nevertheless, it is clear that hexamers with different stoichiometries can form and are capable of hydrolysing ATP (Figure 6). The mass spectrometry data clearly show that the hexamers analysed were mixed, but the mass and stoichiometry of the hexameric fraction does not provide evidence for hexameric ring arrangement of the monomers. However, the modelling of the AUC data argues in favour of hexameric rings.

DISCUSSION

Cellular complexes that contain and depend on RuvBL1 and RuvBL2 are remarkably diverse. Understanding the intrinsic oligomerisation properties of the proteins and their ability to self-assemble would provide the basis for future studies of their functional forms in the cell and the regulation of their function. AUC velocity data of RuvBL1, RuvBL2 and their complex and the modelling of sedimentation coefficients provided quantitative evidence for the subunit composition of their oligomers. Although monomers were predominant in the absence of co-factors, each of RuvBL1 and RuvBL2 also formed stable dimers, trimers and hexamers as minor species. Both AUC and SEC showed that RuvBL2 hexamers were formed in the presence of adenine nucleotides and Mg^{2+} while RuvBL1 remained unchanged. The RuvBL1/2 complex showed a complex profile with a predominant double hexamer. The AUC data suggest that the assembly pathway to the dodecamer involves monomers, dimers, trimers and hexamers as intermediates. Because tetramer and pentamer are not seen, this indicates that hexamers are formed by a sequential mechanism based on the addition of monomer subunits. The monomer, dimer and trimer forms coexist as stable species, while the formation of tetramer or pentamer appears to be kinetically less stable and will quickly progress to the hexamer. The observation of intermediate oligomers between monomer and dodecamer by AUC and SEC is of interest because of the absence of rapid exchange between these forms. This could be due to the heterogeneity of the complexes formed (see below). Slow interconversion between oligomers could also indicate the need for an activation mechanism to promote these exchanges. For RuvBL2, this is provided by ADP or ATP. For both proteins, this is provided by forming the double hexameric complex. While the modelling confirmed the RuvBL1 and RuvBL2 stoichiometries deduced from the *c(s)* fits, the modelling does not distinguish between two homohexamers or two heterohexamers forming the dodecamer. The similar sedimentation coefficients for the RuvBL1 and RuvBL2 oligomers (Table 1) indicate that the individual proteins have similar solution structures, and that these are maintained after addition of nucleotide cofactors.

The presence of mixed RuvBL1/2 hexamers was first suggested by observations in SEC experiments (Figure 1). Mass spectrometry provided direct evidence that the complexes contain mixed hexamers (Figure 8). SEC was used to separate hexamers and dodecamers with appropriate buffer exchange (Experimental). Despite the presence of a dodecamer peak in the SEC profile, double hexamers were not seen by mass spectrometry in the corresponding fractions. Instead, all fractions showed identical spectra for hexamers. It is suspected that the double hexamers were unstable due to the high ionic strength of the buffer used. This indicates that the mixed hexamers characterised originate from the dodecameric complex. In all experiments consistent levels of ATPase activity were measured demonstrating the enzymatic competence of the complexes. This suggests that the close similarity between the two proteins makes them structurally as well as enzymatically interchangeable in the complex. But they are individually essential in all eukaryotes [6, 8-9] and their inability to substitute for each other underlines other dimensions of their specialised functions in vivo.

The observation of mixed hexamers with different stoichiometries was unexpected (Table 2). The biological significance of such complexes is not clear.

Careful examination of the yeast INO80 complex showed a 6:6 Rvb1:Rvb2 ratio [12] but the stoichiometry of other complexes has not been determined. Given the variety of functions associated with RuvBL1 and RuvBL2 as a complex as well as individually [8, 25-26], other structures may exist in vivo. The structural heterogeneity of the yeast complex has been noted and it was suggested that "double and single hexameric rings and even homo-and hetero-oligomers could represent different functional states of these proteins" [31]. The ability of RuvBL1 and RuvBL2 to form complexes with different compositions suggests that different complexes could form in vivo and perform different functions. The composition of the complexes must be tightly controlled. The reconstitution experiments in this study point to a role of ATP in modulating the assembly of mixed hexamers. This is one of several factors that could explain the different structures that were characterised, as discussed in [47]. Post-translational co-regulation of RuvBL1 and RuvBL2 expression in cell cultures was recently observed [48]. This could be necessary for maintaining the assembly of complexes containing equimolar ratios of RuvBL1 and RuvBL2. It was also noted that depletion of one of the proteins depletes the other [16, 48-49] and that overexpression of either RuvBL1 or RuvBL2 could not be achieved in HeLa cells [16]. These results suggest that the predominant form in the cells is an equimolar RuvBL1/2 complex.

The dodecameric human RuvBL1/2 complex studied by EM was assembled from purified RuvBL2-His_6 and partially purified untagged RuvBL1 [5]. In the EM reconstruction major structural differences between the top and bottoms rings were observed and the simplest explanation proposed was a model of two homomeric rings in the complex [5]. However, in view of the mass spectrometry data showing mixed hexamers, the structural differences between the two rings are more likely due to conformational differences. Equimolar amounts of the two proteins were observed in the dodecameric fraction [5], consistent with a 3:3 stoichiometry in the rings, although heterogeneity of the samples could not be excluded.

The three dimensional reconstructions of the human [5] and yeast [31] RuvBL1/2 complexes are significantly different. In the yeast head-to-head model, the two hexamers interact via Domain II contacts. The human complex is best represented by a stacked head-to-tail configuration of the two hexameric rings. While a tail-to-tail configuration is also possible, a head-to-head arrangement could not be fitted (P. Wendler, unpublished observations). This may reflect genuine differences between the yeast and human proteins. However, it seems more likely that different complexes may have been assembled and examined. Our results show that the removal of most of Domain II still allowed the assembly of dodecameric complexes, accompanied with a synergistic increase in ATPase activity. A recent crystallographic report of the human RuvBL1/2 complex using proteins that both lack the globular region of Domain II, also showed a double hexamer [50]. The ΔRuvBL1/ΔRuvBL2 dodecamer clearly argue against a model in which the two hexamer interact primarily via Domain II. However, the deletion of Domain II of RuvBL1 destabilised the dodecamer indicating that some interactions between the hexameric rings involve the globular part of Domain II of RuvBL1. Domain II of RuvBL2 had no effect on the formation of the dodecamer but our observations indicate that the nucleotide-dependent hexamerisation of RuvBL2 is regulated by Domain II. Conformational changes of Domain II may be important for the mechanism of action of RuvBL1/2 and their interactions with other proteins. The globular region of Domain II is connected to

Domain I by two extended β-strands that may allow movement [7]. Such movement of Domain II during the ATP hydrolysis cycle is supported by conformational changes within the complex seen in the two yeast EM studies [31-32]. Domain II movements upon ATP hydrolysis may explain how the RuvBL1/2 proteins are able to restructure protein complexes and modulate protein-protein interactions, such as in the telomerase complex [16], microtubule dynamics [17], or snoRNP maturation [51].

Different structural forms of the RuvBL1/2 complex could underpin its functional diversity and may reflect the acquisition of novel functions in the evolution between yeast and mammals. For example, interactions with c-Myc in higher eukaryotes were mapped to RuvBL1 Domain II [4]. The Zebrafish *liebeskummer* mutation in RuvBL2 (Reptin) which confers a phenotype of heart hyperplasia [26] is caused by an insertion of three amino acid residues in Domain II of RuvBL2 [26]. Factors such as nucleotides, interacting partners, post translational modification associated with protein localisation [52] could regulate the assembly of different complexes through Domain II. Indeed, this may explain how RuvBL1 and RuvBL2 participate in different complexes that antagonistically regulate Wnt dependent transcription [8, 25-26] while they are both essential components of TIP60 [53] and INO80 [13]. RuvBL1/2 complexes isolated from eukaryotic cells will have to be analysed to resolve the existing controversies and higher resolution structures need to be obtained to understand the versatility and function of RuvBL1 and RuvBL2 in multicomponent biological complexes.

AUTHOR CONTRIBUTIONS

Andrew Niewiarowski designed and performed experiments, analysed data and wrote the manuscript; Alison Bradley performed experiments and analysed data; Jayesh Gor performed experiments; Adam McKay and Stephen Perkins performed experiments, calculated models and wrote the manuscript; and Irina Tsaneva designed the study, performed experiments, analysed data and wrote the manuscript.

ACKNOWLEDGEMENTS

We thank Dr Finn Werner and Dr Azubuike Okemefuna in our Department, Dr Petra Wendler (Birkbeck College, London), and Dr Zeynep Baharoglu (Pasteur Institute, Paris) for helpful discussions and experimental assistance.

FUNDING

This work was supported by the Biotechnology and Biological Sciences Research Council, U.K. [BB/E013104/1] and studentship to A.N.

REFERENCES

1 Jha, S. and Dutta, A. (2009) RVB1/RVB2: running rings around molecular biology. Mol. Cell. **34**, 521-533

2 Gallant, P. (2007) Control of transcription by Pontin and Reptin. Trends Cell Biol. **17**, 187-192

3 Zuo, C., Liang, S., Wang, Z., Li, H., Zheng, W. and Ma, W. (2009) Enriching protein-protein and functional interaction networks in human embryonic stem cells. Int. J. Mol. Med. **23**, 811-819

4 Ikura, T., Ogryzko, V. V., Grigoriev, M., Groisman, R., Wang, J., Horikoshi, M., Scully, R., Qin, J. and Nakatani, Y. (2000) Involvement of the TIP60 histone acetylase complex in DNA repair and apoptosis. Cell. **102**, 463-473

5 Puri, T., Wendler, P., Sigala, B., Saibil, H. and Tsaneva, I. R. (2007) Dodecameric structure and ATPase activity of the human TIP48/TIP49 complex. J. Mol. Biol. **366**, 179-192

6 Qiu, X. B., Lin, Y. L., Thome, K. C., Pian, P., Schlegel, B. P., Weremowicz, S., Parvin, J. D. and Dutta, A. (1998) An eukaryotic RuvB-like protein (RUVBL1) essential for growth. J. Biol. Chem. **273**, 27786-27793

7 Matias, P. M., Gorynia, S., Donner, P. and Carrondo, M. A. (2006) Crystal structure of the human AAA+ protein RuvBL1. J. Biol. Chem. **281**, 38918-38929

8 Bauer, A., Chauvet, S., Huber, O., Usseglio, F., Rothbacher, U., Aragnol, D., Kemler, R. and Pradel, J. (2000) Pontin52 and reptin52 function as antagonistic regulators of beta-catenin signalling activity. Embo J. **19**, 6121-6130

9 Kanemaki, M., Kurokawa, Y., Matsu-ura, T., Makino, Y., Masani, A., Okazaki, K., Morishita, T. and Tamura, T. A. (1999) TIP49b, a new RuvB-like DNA helicase, is included in a complex together with another RuvB-like DNA helicase, TIP49a. J. Biol. Chem. **274**, 22437-22444

10 Jin, J., Cai, Y., Yao, T., Gottschalk, A. J., Florens, L., Swanson, S. K., Gutierrez, J. L., Coleman, M. K., Workman, J. L., Mushegian, A., Washburn, M. P., Conaway, R. C. and Conaway, J. W. (2005) A mammalian chromatin remodeling complex with similarities to the yeast INO80 complex. J. Biol. Chem. **280**, 41207-41212

11 Jonsson, Z. O., Dhar, S. K., Narlikar, G. J., Auty, R., Wagle, N., Pellman, D., Pratt, R. E., Kingston, R. and Dutta, A. (2001) Rvb1p and Rvb2p are essential components of a chromatin remodeling complex that regulates transcription of over 5% of yeast genes. J. Biol. Chem. **276**, 16279-16288

12 Shen, X., Mizuguchi, G., Hamiche, A. and Wu, C. (2000) A chromatin remodelling complex involved in transcription and DNA processing. Nature. **406**, 541-544

13 Conaway, R. C. and Conaway, J. W. (2009) The INO80 chromatin remodeling complex in transcription, replication and repair. Trends Biochem. Sci. **34**, 71-77

14 McKeegan, K. S., Debieux, C. M., Boulon, S., Bertrand, E. and Watkins, N. J. (2007) A dynamic scaffold of pre-snoRNP factors facilitates human box C/D snoRNP assembly. Mol. Cell Biol. **27**, 6782-6793

15 Watkins, N. J., Lemm, I., Ingelfinger, D., Schneider, C., Hossbach, M., Urlaub, H. and Luhrmann, R. (2004) Assembly and maturation of the U3 snoRNP in the nucleoplasm in a large dynamic multiprotein complex. Mol. Cell. **16**, 789-798

16 Venteicher, A. S., Meng, Z., Mason, P. J., Veenstra, T. D. and Artandi, S. E. (2008) Identification of ATPases pontin and reptin as telomerase components essential for holoenzyme assembly. Cell. **132**, 945-957

17 Ducat, D., Kawaguchi, S., Liu, H., Yates, J. R., 3rd and Zheng, Y. (2008) Regulation of microtubule assembly and organization in mitosis by the AAA+ ATPase Pontin. Mol. Biol. Cell. **19**, 3097-3110
18 Gartner, W., Rossbacher, J., Zierhut, B., Daneva, T., Base, W., Weissel, M., Waldhausl, W., Pasternack, M. S. and Wagner, L. (2003) The ATP-dependent helicase RUVBL1/TIP49a associates with tubulin during mitosis. Cell Motil. Cytoskeleton. **56**, 79-93
19 Sigala, B., Edwards, M., Puri, T. and Tsaneva, I. R. (2005) Relocalization of human chromatin remodeling cofactor TIP48 in mitosis. Exp Cell Res. **310**, 357-369
20 Vogelstein, B. and Kinzler, K. W. (2004) Cancer genes and the pathways they control. Nat. Med. **10**, 789-799
21 Huber, O., Menard, L., Haurie, V., Nicou, A., Taras, D. and Rosenbaum, J. (2008) Pontin and reptin, two related ATPases with multiple roles in cancer. Cancer Res. **68**, 6873-6876
22 Ruhl, D. D., Jin, J., Cai, Y., Swanson, S., Florens, L., Washburn, M. P., Conaway, R. C., Conaway, J. W. and Chrivia, J. C. (2006) Purification of a human SRCAP complex that remodels chromatin by incorporating the histone variant H2A.Z into nucleosomes. Biochemistry. **45**, 5671-5677
23 Gstaiger, M., Luke, B., Hess, D., Oakeley, E. J., Wirbelauer, C., Blondel, M., Vigneron, M., Peter, M. and Krek, W. (2003) Control of nutrient-sensitive transcription programs by the unconventional prefoldin URI. Science. **302**, 1208-1212
24 Jonsson, Z. O., Jha, S., Wohlschlegel, J. A. and Dutta, A. (2004) Rvb1p/Rvb2p recruit Arp5p and assemble a functional Ino80 chromatin remodeling complex. Mol. Cell. **16**, 465-477
25 Kim, J. H., Kim, B., Cai, L., Choi, H. J., Ohgi, K. A., Tran, C., Chen, C., Chung, C. H., Huber, O., Rose, D. W., Sawyers, C. L., Rosenfeld, M. G. and Baek, S. H. (2005) Transcriptional regulation of a metastasis suppressor gene by Tip60 and beta-catenin complexes. Nature. **434**, 921-926
26 Rottbauer, W., Saurin, A. J., Lickert, H., Shen, X., Burns, C. G., Wo, Z. G., Kemler, R., Kingston, R., Wu, C. and Fishman, M. (2002) Reptin and pontin antagonistically regulate heart growth in zebrafish embryos. Cell. **111**, 661-672
27 Diop, S. B., Bertaux, K., Vasanthi, D., Sarkeshik, A., Goirand, B., Aragnol, D., Tolwinski, N. S., Cole, M. D., Pradel, J., Yates, J. R., 3rd, Mishra, R. K., Graba, Y. and Saurin, A. J. (2008) Reptin and Pontin function antagonistically with PcG and TrxG complexes to mediate Hox gene control. EMBO Rep. **9**, 260-266
28 Lupas, A. N. and Martin, J. (2002) AAA proteins. Curr. Opin. Struct. Biol. **12**, 746-753
29 Neuwald, A. F., Aravind, L., Spouge, J. L. and Koonin, E. V. (1999) AAA+: A class of chaperone-like ATPases associated with the assembly, operation, and disassembly of protein complexes. Genome Res. **9**, 27-43
30 Putnam, C. D., Clancy, S. B., Tsuruta, H., Gonzalez, S., Wetmur, J. G. and Tainer, J. A. (2001) Structure and mechanism of the RuvB Holliday junction branch migration motor. J. Mol. Biol. **311**, 297-310
31 Torreira, E., Jha, S., Lopez-Blanco, J. R., Arias-Palomo, E., Chacon, P., Canas, C., Ayora, S., Dutta, A. and Llorca, O. (2008) Architecture of the pontin/reptin complex, essential in the assembly of several macromolecular complexes. Structure. **16**, 1511-1520
32 Gribun, A., Cheung, K. L., Huen, J., Ortega, J. and Houry, W. A. (2008) Yeast Rvb1 and Rvb2 are ATP-Dependent DNA Helicases that Form a Heterohexameric Complex. J. Mol. Biol. **376**, 1320-1333

33 Laue, T. M., Shah, B. D., Ridgeway, T. M. and Pelletier, S. L. (1992) Computer-aided interpretation of analytical sedimentation data for proteins. Analytical Ultracentrifugation in Biochemistry and Polymer Science, 90-125
34 Perkins, S. J. (1986) Protein volumes and hydration effects. The calculations of partial specific volumes, neutron scattering matchpoints and 280-nm absorption coefficients for proteins and glycoproteins from amino acid sequences. Eur. J. Biochem. **157**, 169-180
35 Balbo, A. S., ed. (2005) Analytical ultracentrifugation in the study of protein self-association and heterogeneous protein-protein interactions. Cold Spring Harbor Laboratory Press, New York, NY.
36 Schuck, P. (2000) Size-distribution analysis of macromolecules by sedimentation velocity ultracentrifugation and lamm equation modeling. Biophys. J. **78**, 1606-1619
37 Nan, R., Gor, J. and Perkins, S. J. (2008) Implications of the progressive self-association of wild-type human factor H for complement regulation and disease. J. Mol. Biol. **375**, 891-900
38 Garcia De La Torre, J., Huertas, M. L. and Carrasco, B. (2000) Calculation of hydrodynamic properties of globular proteins from their atomic-level structure. Biophys. J. **78**, 719-730
39 Perkins, S. J., Okemefuna, A. I., Nan, R., Li, K. and Bonner, A. (2009) Constrained solution scattering modelling of human antibodies and complement proteins reveals novel biological insights. J. R. Soc. Interface. **6 Suppl 5**, S679-696
40 Garcia de la Torre, J., Llorca, O., Carrascosa, J. L. and Valpuesta, J. M. (2001) HYDROMIC: prediction of hydrodynamic properties of rigid macromolecular structures obtained from electron microscopy images. Eur. Biophys. J. **30**, 457-462
41 McKay, A. R., Ruotolo, B. T., Ilag, L. L. and Robinson, C. V. (2006) Mass measurements of increased accuracy resolve heterogeneous populations of intact ribosomes. J. Am. Chem Soc. **128**, 11433-11442
42 Felitsyn, N., Kitova, E. N. and Klassen, J. S. (2001) Thermal decomposition of a gaseous multiprotein complex studied by blackbody infrared radiative dissociation. Investigating the origin of the asymmetric dissociation behavior. Anal. Chem. **73**, 4647-4661
43 Jurchen, J. C. and Williams, E. R. (2003) Origin of asymmetric charge partitioning in the dissociation of gas-phase protein homodimers. J. Am. Chem. Soc. **125**, 2817-2826
44 Benesch, J. L., Aquilina, J. A., Ruotolo, B. T., Sobott, F. and Robinson, C. V. (2006) Tandem mass spectrometry reveals the quaternary organization of macromolecular assemblies. Chem. Biol. **13**, 597-605
45 Ruotolo, B. T., Hyung, S. J., Robinson, P. M., Giles, K., Bateman, R. H. and Robinson, C. V. (2007) Ion mobility-mass spectrometry reveals long-lived, unfolded intermediates in the dissociation of protein complexes. Angew Chem. Int. Ed. Engl. **46**, 8001-8004
46 Wysocki, V. H., Jones, C. M., Galhena, A. S. and Blackwell, A. E. (2008) Surface-induced dissociation shows potential to be more informative than collision-induced dissociation for structural studies of large systems. J. Am. Soc. Mass Spectrom. **19**, 903-913
47 Cheung, K. L., Huen, J., Houry, W. A. and Ortega, J. (2010) Comparison of the multiple oligomeric structures observed for the Rvb1 and Rvb2 proteins. Biochem. Cell Biol. **88**, 77-88

48 Haurie, V., Menard, L., Nicou, A., Touriol, C., Metzler, P., Fernandez, J., Taras, D., Lestienne, P., Balabaud, C., Bioulac-Sage, P., Prats, H., Zucman-Rossi, J. and Rosenbaum, J. (2009) Adenosine triphosphatase pontin is overexpressed in hepatocellular carcinoma and coregulated with reptin through a new posttranslational mechanism. Hepatology. **50**, 1871-1883

49 Gospodinov, A., Tsaneva, I. and Anachkova, B. (2009) RAD51 foci formation in response to DNA damage is modulated by TIP49. Int. J. Biochem. Cell Biol. **41**, 925-933

50 Gorynia, S., Matias, P. M., Bandeiras, T. M., Donner, P. and Carrondo, M. A. (2008) Cloning, expression, purification, crystallization and preliminary X-ray analysis of the human RuvBL1-RuvBL2 complex. Acta Crystallogr. Sect. F Struct. Biol. Cryst. Commun. **64**, 840-846

51 Watkins, N. J., Dickmanns, A. and Luhrmann, R. (2002) Conserved stem II of the box C/D motif is essential for nucleolar localization and is required, along with the 15.5K protein, for the hierarchical assembly of the box C/D snoRNP. Mol. Cell Biol. **22**, 8342-8352

52 Kim, J. H., Choi, H. J., Kim, B., Kim, M. H., Lee, J. M., Kim, I. S., Lee, M. H., Choi, S. J., Kim, K. I., Kim, S. I., Chung, C. H. and Baek, S. H. (2006) Roles of sumoylation of a reptin chromatin-remodelling complex in cancer metastasis. Nat. Cell Biol. **8**, 631-639

53 Doyon, Y. and Cote, J. (2004) The highly conserved and multifunctional NuA4 HAT complex. Curr. Opin. Genet Dev. **14**, 147-154

Biochemical Journal Immediate Publication. Published on 22 Apr 2010 as manuscript BJ20100489

OLIGOMER	MONOMER	DIMER	TRIMER	HEXAMER	INTERMEDIATE	DODECAMER
Number of experiments	11	11	11	10	9	
His_6-RuvBL1 sequence mass (kDa)	52	105	157	314	471	628
His_6-RuvBL1 *c(M)* mass (kDa)	49 ± 8	97 ± 20	169 ± 36	299 ± 30	491 ± 79	n.o.
His_6-RuvBL1 *c(s)* (S)	3.0 ± 0.1	4.7 ± 0.4	6.8 ± 0.5	10.1 ± 0.4	14.2 ± 0.5	n.o.
Number of experiments	31	29	27	29	16	
RuvBL2-His_6 sequence mass (kDa)	52	104	156	313	469	616
RuvBL2-His_6 *c(M)* mass (kDa)	47 ± 14	92 ± 24	160 ± 39	303 ± 76	500 ± 104	n.o.
RuvBL2-His_6 *c(s)* (S)	3.0 ± 0.2	4.7 ± 0.3	6.9 ± 0.4	10.3 ± 0.4	14.8 ± 0.5	n.o.
Number of experiments	11	11	11	11	11	11
RuvBL1-His_6 /RuvBL2 sequence mass (kDa)	51	102	153	307	460	614
RuvBL1-His_6 /RuvBL2 *c(M)* mass (kDa)	72 ± 9	154 ± 14	265 ± 35	406 ± 78	594 ± 133	975 ± 196
RuvBL1-His_6 /RuvBL2 *c(s)* (S)	3.2 ± 0.2	5.2 ± 0.2	7.3 ± 0.3	10.3 ± 0.2	13.0 ± 0.5	18.4 ± 0.4
Modelled sedimentation coefficient Hexamer 1 (S)	3.3	5.2	6.8	10.6	9mer = 14.7	18.4
Modelled sedimentation coefficient Hexamer 2 (S)	3.3, 3.7	5.6	7.2	11.5	n.o.	n.o.

Table 1. Summary of AUC interference data analyses by SEDFIT. n.o.- not observed

Biochemical Journal Immediate Publication. Published on 22 Apr 2010 as manuscript BJ20100489

Protein or Protein Complex	Experimentally Measured Mass / (Da)	Expected Mass / (Da)	Adduct Corrected Mass / (Da) [41]
Hexameric RuvBL1-His_6/RuvBL2 (4:2)	313,682 ± 40	312,047	313, 029
Hexameric RuvBL1-His_6/RuvBL2 (3:3)	311,934 ± 19	310,770	311, 509
RuvBL1-His_6	52,580 ± 12	52,433.4	-
RuvBL2	51,047 ± 13	51,156.5	-
Pentameric RuvBL1-His_6/RuvBL2 (3:2)	260,850 ± 13	259,613	260, 351
Pentameric RuvBL1-His_6/RuvBL2 (4:1)	262,360 ± 11	260,890-	261, 871
Peptide Fragment	9,666 ± 1	B_{96} 9,636	-
RuvBL1-His_6/RuvBL2 (4:2) minus peptide	303,648 ± 83	302,411	-
ΔRuvBL1/RuvBL2 (3:3)	242,730 ± 21	240,625	242, 543
ΔRuvBL1-His_6/ΔRuvBL2 (4:2)	243,165 ± 7	241,481	243, 542
ΔRuvBL1-His_6/ΔRuvBL2 (5:1)	244, 938 ± 22	242,336	244, 540

Table 2: Summary of experimental and theoretical masses of RuvBL1, RuvBL2 and complexes

FIGURE LEGENDS

Figure 1. Oligomerisation of the RuvBL1/2 complex by SEC.

(**A)** RuvBL1-His_6 and RuvBL2 captured on Talon column were fractionated by SEC on Superose 6 HR column. 280 nm UV absorbance curves are shown (**B)** Fractions 13 and 14 (from **A**) were re-applied to the column at different protein concentrations; the dotted line represents the expected elution volume of a dodecamer of RuvBL1/2. (**C)** The peak fraction of the complex was dialysed against buffers containing either 0.5 mM EDTA or 2 mM $MgCl_2$ and the sample in $MgCl_2$ was incubated with 0.5 mM ATP and analysed by SEC. (**D**) The hexameric complex from fraction 15 (from **A**) was re-applied to the column and again eluted as a hexamer; the dotted line indicates the expected elution volume of a single hexamer of RuvBL1/2. Fractions 14-16 (from **D**) were captured on a Talon resin and eluted with imidazole. The numbered arrows in each figure show the elution volumes of four molecular mass standards in kDa and the void volume (V_0). (**E)** SEC fractions 12 to 16 (from **D**) and the eluant from the Talon resin (Talon) were analysed by 12 % SDS PAGE and stained with silver;

Figure 2. *c(s)* distribution analyses of sedimentation velocity data for RuvBL1, RuvBL2 and their complex.

The *c(s)* fits show one in five boundary scans for reason of clarity. Arrows indicate the $s^0_{20,w}$ value for each discrete peak calculated using SEDFIT and observed in representative interference optics data sets at rotor speeds of 30,000 r.p.m. for individual proteins and 25,000 r.p.m. for the RuvBL1/2 complex. *c(s)* distributions are shown for (**A)** His_6-RuvBL1 at 0.8 mg/ml in 0.1 mM EDTA; (**B)** His_6-RuvBL1 at 1.5 mg/ml in 2 mM Mg and 0.5 mM ATP; (**C)** RuvBL2-His_6 at 1.2 mg/ml in 0.1 mM EDTA; (**D)** RuvBL2-His_6 at 0.8 mg/ml in 2 mM Mg and 0.5 mM ATP; (**E)** the RuvBL1-His_6/2 complex at 0.8 mg/ml in 0.1 mM EDTA; (**F)** the RuvBL1-His_6/2 complex at 0.5 mg/ml in 2 mM Mg and 0.5 mM ATP.

Figure 3. Concentration dependence of the sedimentation coefficients for RuvBL1, RuvBL2 and their complex by SEDFIT.

The three panels summarise the corresponding SEDFIT analyses for (**A)** RuvBL1-His_6, (**B)** His_6-RuvBL2, and (**C)** the RuvBL1-His_6/RuvBL2 Complex. The fitted regression lines indicate the average sedimentation coefficients for each observed species. The symbols in alternation (▼;▽;▲;△;◆;◇) show the distinct oligomeric species that were clearly resolved in each *c(s)* plot. The number of monomers assigned to each peak is shown at the right (either 1, 2, 3, 6, 9 or 12) (**D, E, F**). These data are summarised in Table 1.

Figure 4. Oligomeric forms of RuvBL1 used for modelling predictions of the sedimentation coefficients.

The predicted sedimentation coefficient from each model is shown in brackets. In the top row, side views show the monomers in the dimer and trimer as orange, blue and green ribbon traces. The electron microscopy map of the RuvBL1/2 complex is superimposed onto the dodecamer head-to-tail model. In the middle row, the side view of the hexamer is shown in magenta with the six bound ADP molecules in blue. The addition of trimers to form either the nonamer or dodecamer used the same colours in the top row. In the bottom row, the hexamer and electron microscopy models are rotated by 90° to reveal the void at the middle of the hexamer.

Figure 5. Size exclusion chromatography of ΔRuvBL2-His$_6$.

Fractionation of purified ΔRuvBL2-His$_6$ by SEC on Superose 6 HR. (**A)** The UV absorbance curves (280 nm) are shown for ΔRuvBL2-His$_6$ with EDTA or Mg-ATP and full length RuvBL2-His$_6$ in EDTA, as indicated. (**B)** The elution profiles of ΔRuvBL2-His$_6$ at three protein concentrations, as indicated. The dotted line shows the expected elution volume of a monomer. The numbered arrows in each figure show the elution volumes of four molecular mass standards in kDa and the void volume (V_0). Below, the deletion in Domain II modelled on the structure of RuvBL1

Figure 6. Oligomerisation and ATPase activity of RuvBL1/2 complexes containing deletion mutants.

Fractionation of RuvBL1/2 oligomers by Superose 6 HR SEC shown as UV absorbance traces for different complexes containing wild type and Domain II deletion mutants (Δ), as indicated (**A, D, G, J**). Fractions were analysed by 12 % polyacrylamide SDS PAGE stained with Coomassie brilliant blue (**B, E, H, K**). Protein concentration and ATPase activity of the fractions (**C, F, I, L**). ATPase activity is defined as the nmoles of ATP hydrolysed after 30 minutes incubation at 37 ºC in a 200 µl reaction.

Figure 7. Reconstitution of RuvBL1/2 complexes and effect of ATP

Size exclusion chromatography of complexes reconstituted from purified RuvBL1-His$_6$ and RuvBL2-His$_6$ in EDTA or Mg-ATP buffers, as indicated. RuvBL2 was incubated in the Mg-ATP buffer before addition of RuvBL1. Both mixtures were concentrated before loading on the Superose 6 HR column (Experimental). Control samples of RuvBL1 or RuvBL2 alone, as indicated, were also prepared and analyzed in parallel.

Figure 8. Mass spectrometry of the RuvBL1/RuvBL2 and ΔRuvBL1/ΔRuvBL2 hexameric complexes reveals heterogenous poulations of mixed hexamers.

(A) MS spectrum of the RuvBL1/RuvBL2 complex obtained after separation of the hexameric fraction by SEC on a Superdex 200 column. The predominant ion series centred on 8250 *m/z* has a mass consistent with a 4:2 stoichiometry of RuvBL1/RuvBL2. A second smaller ion series in the spectrum labelled * is centred on 8197 *m/z* and has a mass consistent with 3:3 stoichiometry of RuvBL1/RuvBL2.

(B) The tandem MS spectrum of the 39+ charge state. Fragmentation of this ion confirms the 4:2 stoichiometry and the presence of both RuvBL proteins in the hexamer producing three related fragment ion families. The ion series labelled (1) in the spectrum results from the fragmentation of the 39+ hexameric ion to produce highly charged RuvBL1 monomer ions centred on 2020 *m/z* and ions from a pentameric RuvBL1/RuvBL2 complex with a stoichiometry of 3:2. Similarly, the ion series labelled (2) results from the fragmentation of the 39+ charge state of the 4:2 hexamer to produce highly charged RuvBL2 monomer ions centred on 2040 m/z and and ions from a pentameric RuVBL1/RuvBL2 complex with a stoichiometry of 4:1. The final ion series labelled (3) represents the loss of a 9 kDa fragment of RuvBL1, resulting in the formation of a complementary fragment ion of the hexameric complex after loss of this fragment.

(C) The MS spectrum of the hexameric fraction of the ΔRuvBL1/ΔRuvBL2 complex after separation by SEC on a Superdex 200 column. The predominant ion series centred on 7115 *m/z* has a mass consistent with a 4:2 stoichiometry of ΔRuvBL1/ΔRuvBL2. In total three ion series are distinguishable and are visible in the expansion of the spectrum (inset). They are

labelled (a-c) on the 35+ charge state and are consistent with 3:3, 4:2 and 5:1 stoichiometries of ΔRuvBL1/RuvBL2 respectively.

Biochemical Journal Immediate Publication. Published on 22 Apr 2010 as manuscript BJ20100489

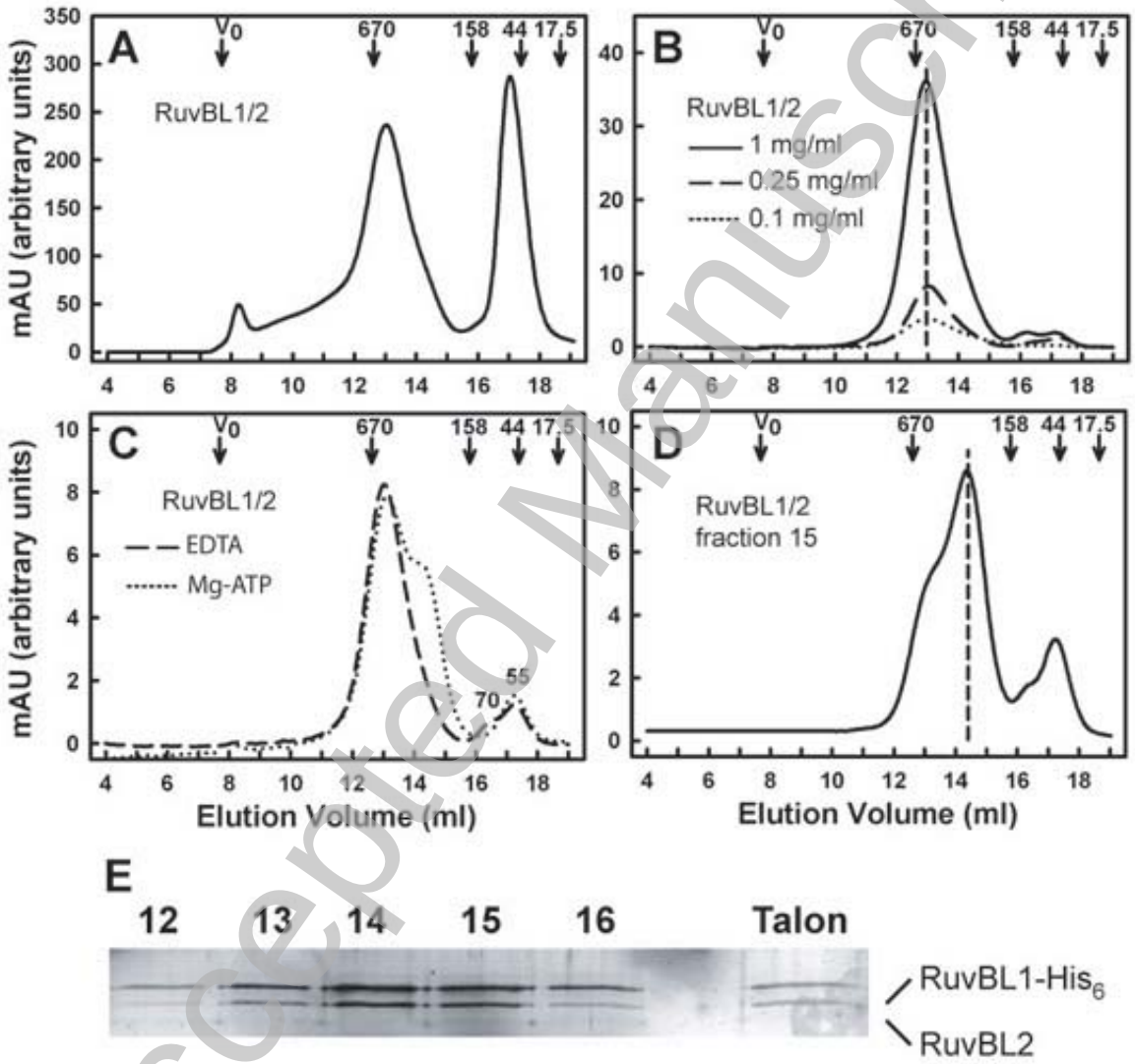

Figure 1

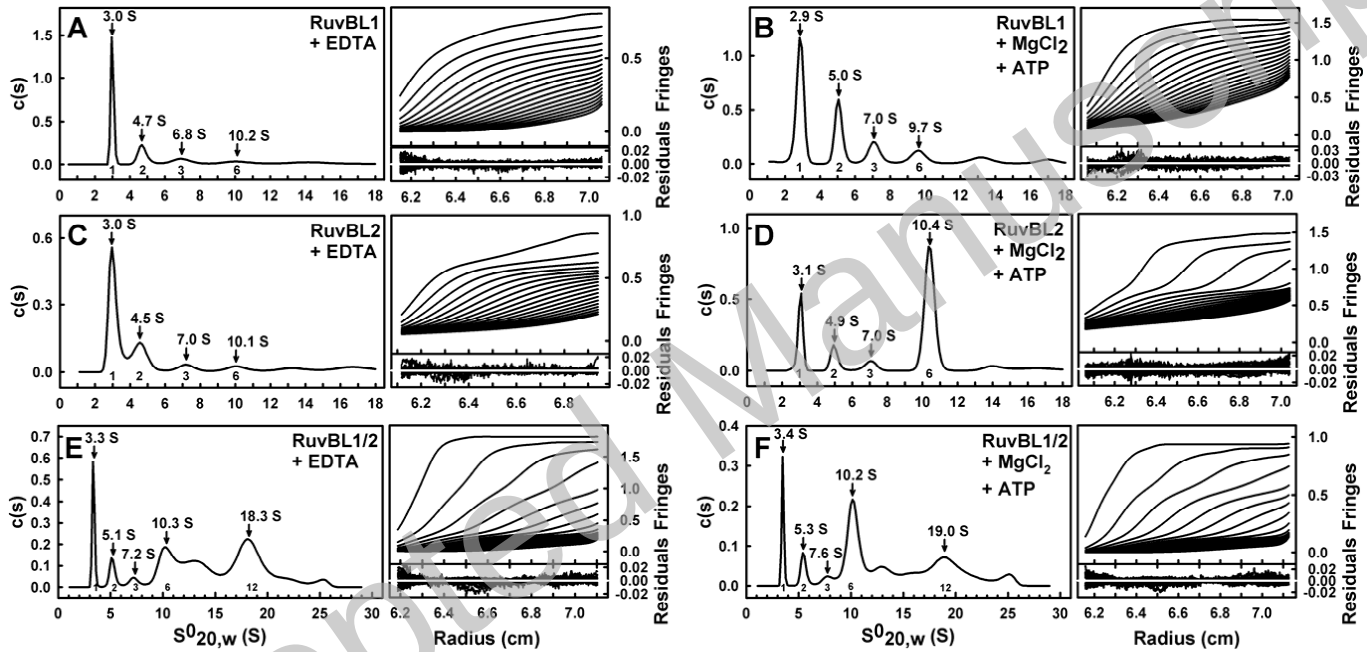

FIGURE 2

Biochemical Journal Immediate Publication. Published on 22 Apr 2010 as manuscript BJ20100489

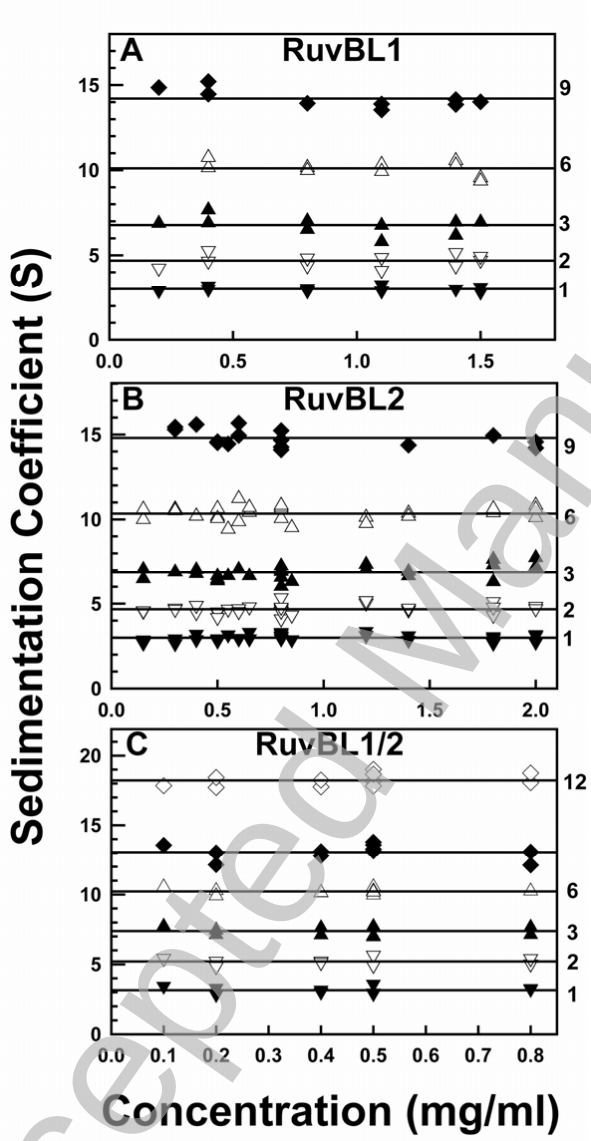

FIGURE 3

Biochemical Journal Immediate Publication. Published on 22 Apr 2010 as manuscript BJ20100489

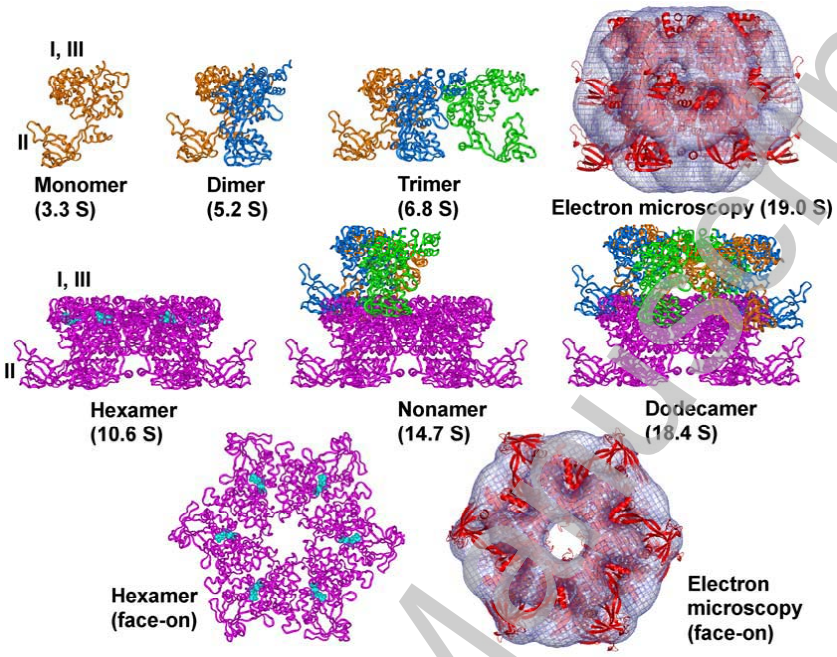

FIGURE 4

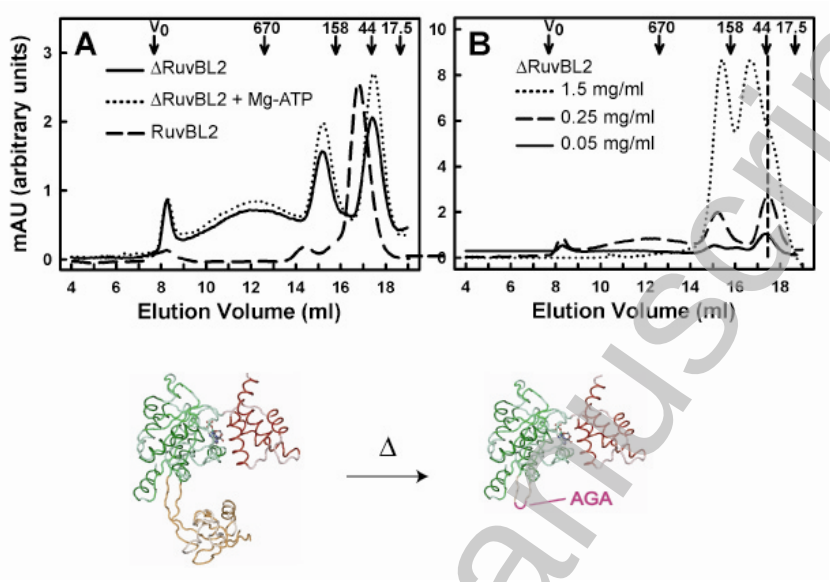

FIGURE 5

Biochemical Journal Immediate Publication. Published on 22 Apr 2010 as manuscript BJ20100489

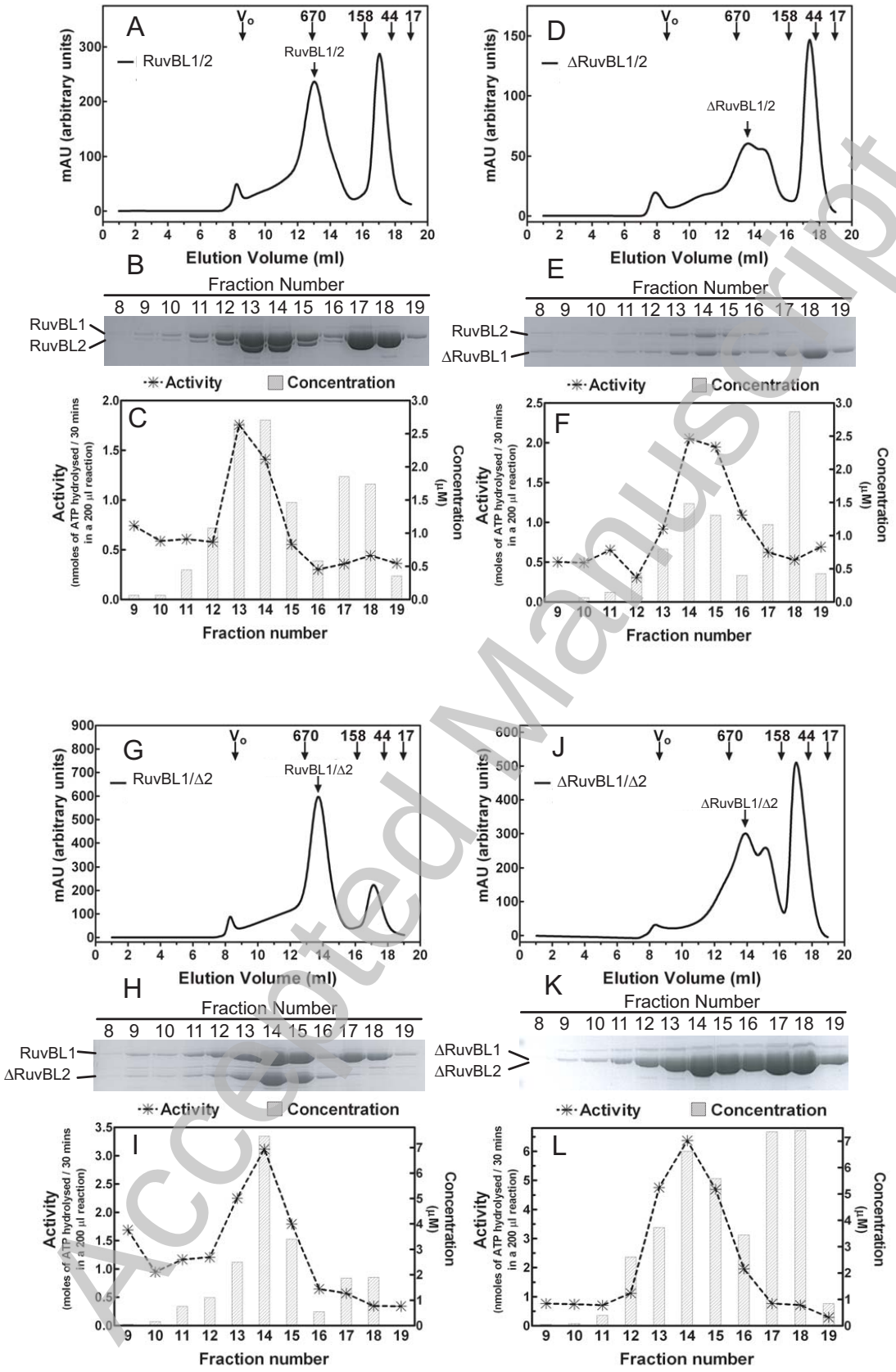

Figure 6

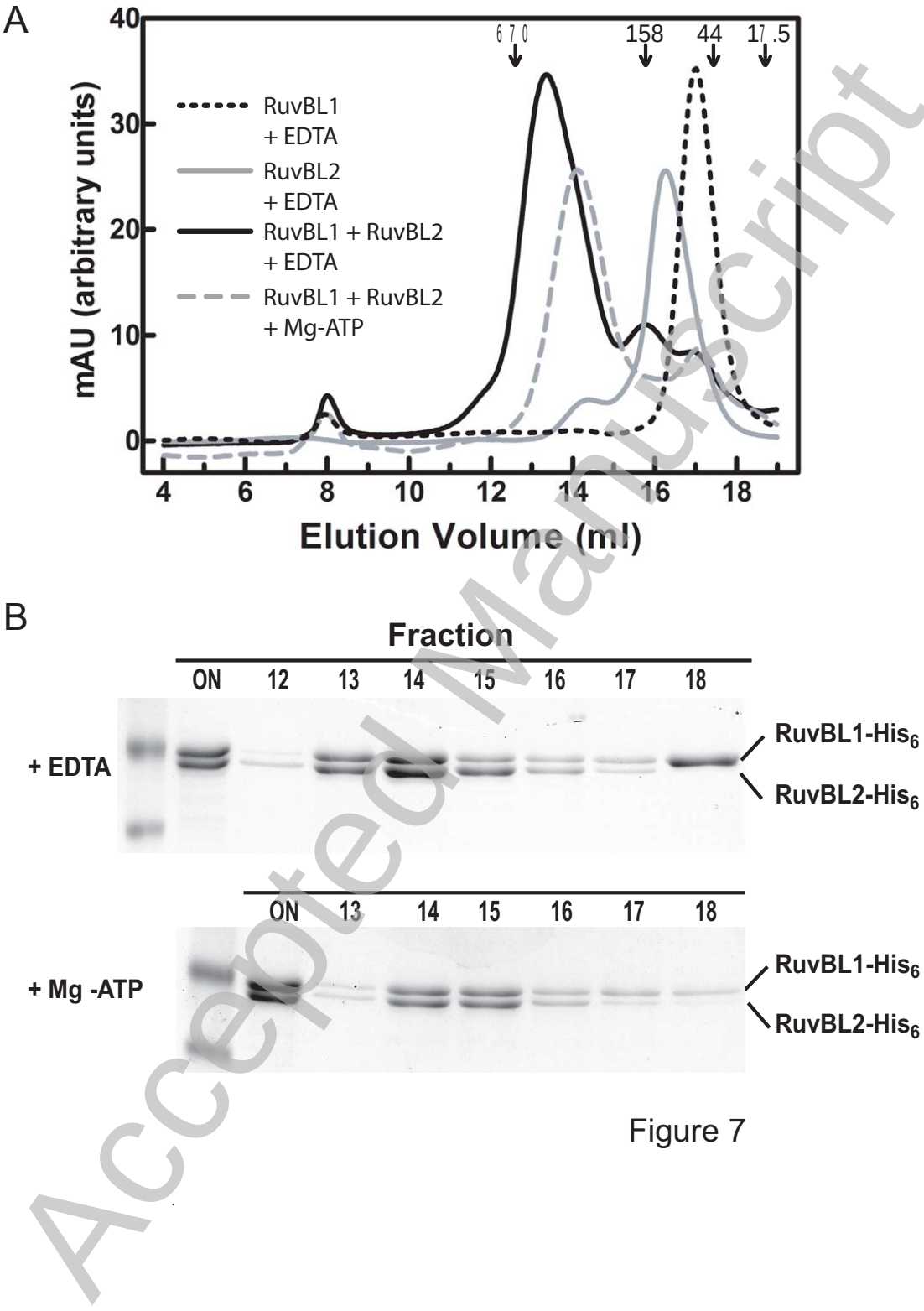

Figure 7

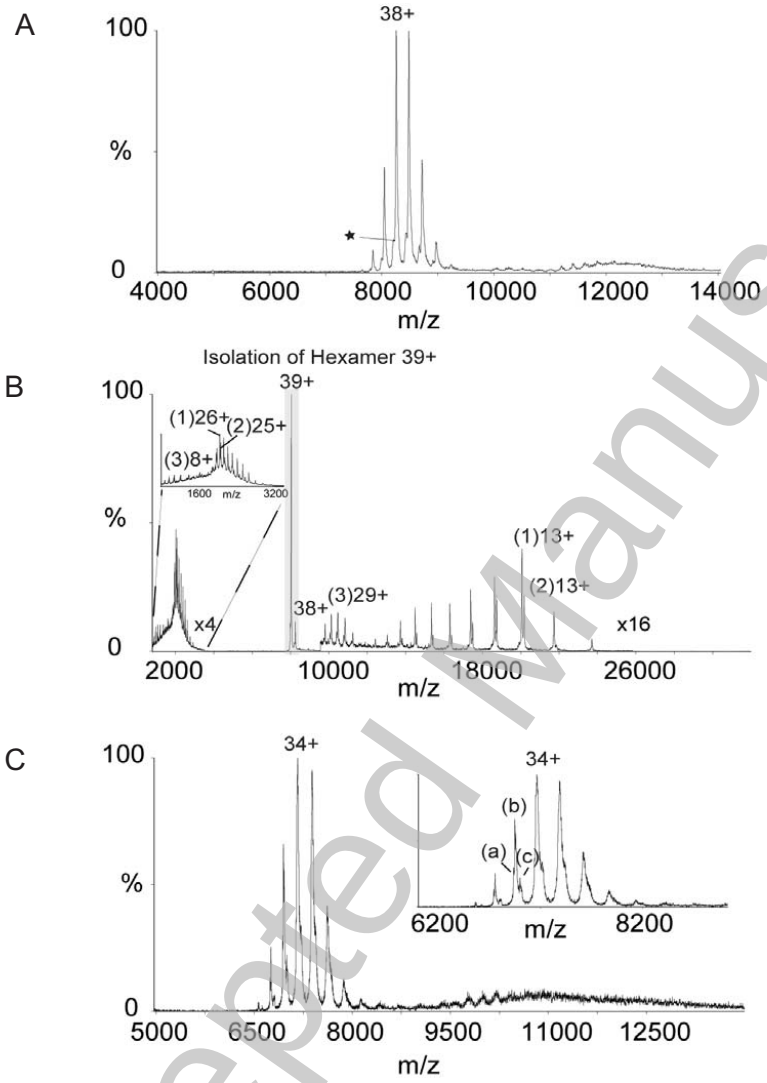

Figure 8